Dynamics of yielding observed in a three-dimensional aqueous dry foam

Florence Rouyer, Sylvie Cohen-Addad, Michèle Vignes-Adler, and Reinhard Höhler
Laboratoire de Physique des Matériaux Divisés et des Interfaces, UMR 8108 du CNRS, Université de Marne-la-Vallée, 5 Boulevard Descartes, 77454 Marne-la-Vallée cedex 2, France

(Received 25 June 2002; revised manuscript received 22 November 2002; published 24 February 2003)

We study the onset of yielding in stable three-dimensional dry foams following the start up of steady shear flow. By means of a charge-coupled device camera equipped with a small depth-of-field objective, we visualize the Plateau border network in the bulk of the foam. The onset of yielding is identified with the deformation γ_c for which shear induced rearrangements start occurring. We show that γ_c is independent of shear rate $\dot{\gamma}$ in a quasistatic regime whereas at high strain rates, a rapid increase of γ_c with $\dot{\gamma}$ is observed, in qualitative agreement with theoretical models. Moreover, spatiotemporal image analyses are used to determine the velocity profile in the gap. We find that this profile remains linear up to strains far beyond γ_c. Moreover, we have studied the strain history dependence of γ_c.

DOI: 10.1103/PhysRevE.67.021405 PACS number(s): 82.70.−y, 62.20.Fe, 83.80.Iz

I. INTRODUCTION

Aqueous foams are concentrated dispersions of gas bubbles in a surfactant solution. Even though they are only made of fluids, foams behave elastically under small applied stresses, whereas when subjected to large stresses they flow like viscous non-Newtonian liquids. The crossover between these two types of behavior is called yielding. In the context of macroscopic rheological measurements, the yield strain is usually defined as the strain corresponding to the maximum of stress obtained in a strain growth experiment [1]. At the scale of the individual bubbles, yielding may be defined as the crossover from reversible elastic behavior to a regime where the deformation involves topological changes of the bubble packing [1,2].

The first theoretical analysis of yielding in foams and concentrated emulsions is due to Princen [3]. Based on the observation that this rheological behavior is common to a large class of complex fluids, recent theoretical models have attempted to identify a general framework providing a link between the macroscopic rheological response and the local structural changes that accompany the yielding process under quasistatic conditions [4]. In these models, the strength of the coupling between the rearrangements in neighboring ''mesoscopic regions'' plays an important role. Numerical simulations of steady shear flow in foam often rely on simplified descriptions of the structure and the interactions between bubbles: Simulations based on the vertex model exhibit avalanches of rearrangements [5], whereas using the bubble model local rearrangements are predicted [6]. The surface evolver software, allows to carry out highly accurate three-dimensional (3D) simulations, but only in the quasistatic regime [2,7]. Concerning the dynamics of yielding, several 2D theoretical studies and simulations have shown that under large strain rates, viscous forces in the foam strongly affect yielding behavior [8–11]. Since the pioneering work of Khan *et al.*, yielding of 3D foams has been studied on the macroscopic scale by rheological measurements [12–15]. The dynamics of bubble rearrangements in wet foams that undergo yielding have been studied using diffusing-wave spectroscopy. This work has confirmed the crucial role played by these rearrangements for the rheological behavior [16,17]. Moreover, recent theoretical studies have shown how yielding can be interpreted as a generic jamming phenomenon [18,19].

In this paper, we present direct observations of the local structural changes that accompany the onset of yielding in a 3D dry foam. We report the first measurement of the strain at which shear-induced rearrangement sets in a strain growth experiment. These data are compared to theoretical predictions concerning the influence of the strain rate on yielding.

II. MATERIALS AND METHODS

We have developed a formulation based on well-characterized chemicals allowing to obtain highly stable foams that do not exhibit coalescence under shear. The foaming liquid is an aqueous solution containing a mixture of sodium dodecyl sulfate (SDS), polyethylene oxyde (PEO, $M_w = 3 \times 10^5$ g mol^{-1}), dodecanol, and butanol. The products were all purchased from Aldrich and used as received. The solution is prepared using pure water (MilliQ) as follows: First, 0.02 g of PEO is dissolved in 100 ml of water and subjected to a gentle mechanical agitation for 1 h. Then, 0.006 g of dodecanol is diluted in 5 ml of butanol. This alcoholic solution is added to the PEO solution, and further gently agitated for 15 min. Besides, 0.2 g of SDS is dissolved in 40 ml of water. The final foaming solution is obtained by mixing the PEO solution with the SDS solution and completing with water up to 200 ml. It is gently agitated for 15 min. The final concentrations are SDS 0.1% g/g, PEO 0.01% g/g, dodecanol 0.003% g/g, butanol 2% g/g. To avoid aging effects, the solution is prepared no more than 24 h before use. The surface tension of the foaming solution, σ, was measured by the de Nouÿ method and found to be equal to 23 mN m^{-1} at 20 °C. Its viscosity was determined using an Ostwald capillary viscometer tube at 20 °C, $\mu = 1.08$ mPa s.

The foam is generated by mixing nitrogen gas and the foaming solution using a setup inspired by the one described by Khan [12]. In our device, the gas and the solution are injected at constant flow rates (28 and 2.3 ml/min, respec-

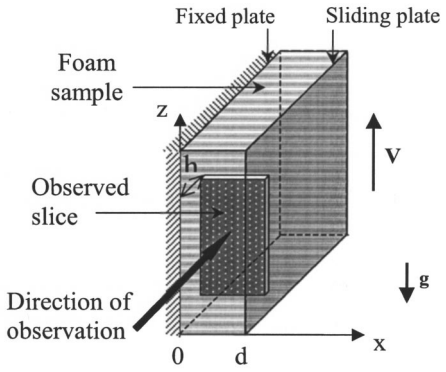

FIG. 1. Experimental setup. The sliding plate cell consists of two parallel plates (100×80 mm^2). The observed slice is situated at a depth ($h=10$ mm) at the midheight of the foam sample and is 2.5 mm thick. The arrows V and g show the directions of the velocity of the moving plate and of gravity, respectively.

tively) at the entrance of a Plexiglass tube (200 mm long, 20 mm inside diameter) filled with compacted glass beads (1.5 mm diameter). The porosity of the bead packing is about 36%. Under these conditions, the gas volume fraction of the generated foam is 92% and the average bubble radius is of the order of 0.1 mm. The output of the generator is connected to a flexible tube, allowing to fill directly a sliding plate cell (cf. Fig. 1). The air in contact with the sample is saturated with humidity. After injection, the foam drains *in situ* for 75 min before the shearing experiment is started. To determine a typical gas volume fraction of the foam at this time, a sample is prepared and injected into a cell whose geometry corresponds to that of the sliding plate cell and which is weighted after 75 min. We also measure the foam volume and thus obtain an average gas volume fraction for the entire sample, it is larger than 99%. The liquid content in the foam sample will be highest near the bottom due to drainage and we expect the gas volume fraction at midheight, where we study the foam, to be above 99%. All the experiments have been carried out at a temperature of (20 ± 1) °C.

A charge-coupled device camera equipped with a very thin depth-of-field objective allows to observe the structure inside the foam. Since it is very dry, the films are so thin that they are almost totally transparent and the only visible elements are the Plateau borders that appear as black lines on the images (cf. Fig. 2). The camera is focused on a region 10 mm inside the foam and captures images of a foam ''slice.'' It is 2.5 mm deep, the width is equal to the gap between the plates and the height is chosen such that the volume of observation, denoted V_{obs}, is equal to 430 mm^3 for all of the experiments at different gap widths. Before applying the shear, the disordered and polydispersed foam structure is inspected; the bubble size is estimated from the bubble contours drawn by the Plateau borders visible on the images [cf. Fig. 2(a)]. This procedure yields an average bubble radius $R=0.8$ mm with a standard deviation of 0.4 mm, the minimum and the maximum radii are equal to 0.2 and 2 mm, respectively. The average bubble size remains constant during the shearing experiment. No film rupture is observed,

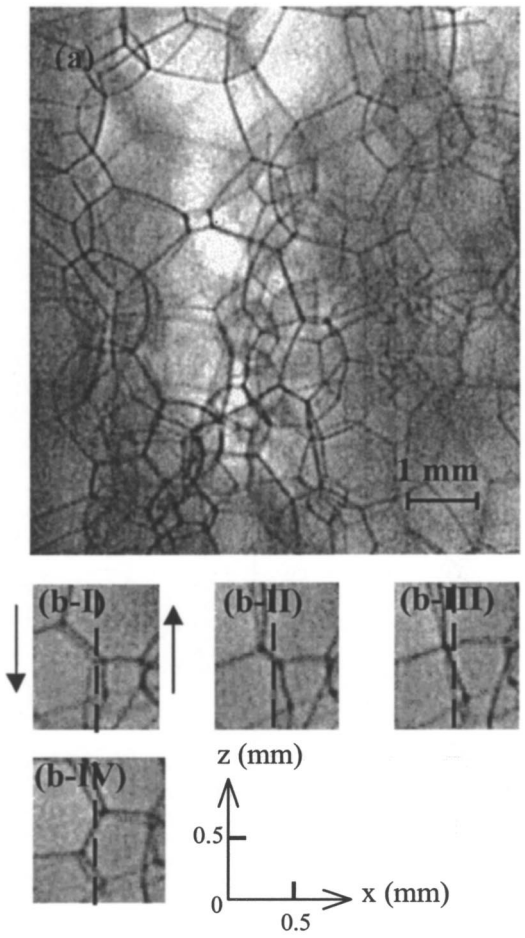

FIG. 2. (a) Part of the image of a quiescent foam slice observed at a depth $h=10$ mm inside the sample. (b) Four successive images showing a topological $T1$ transformation: (b-I) and (b-II) before the $T1$, (b-III) instant of $T1$, (b-IV) after the $T1$. The dotted line indicates a typical pixel line used for constructing spatiotemporal plots.

even during the shearing. The rate of coarsening induced bubble rearrangements slows down considerably during the first 75 min of the foams existence. Indeed, observations on static foam show that right after the production of the sample, of the order of 1% of the bubbles in the observed volume participate in rearrangements during one second, suggesting that the rearranged bulk volume fraction per second is of the order of 10^{-2} s^{-1}. At a foam age of 75 min, this parameter is more than 60 times smaller. Besides the chemical composition and the bubble size distribution described in this paragraph, the rheological response of foams, generally, also depends on strain history [15,17,20]. During foam injection into the sliding plate cell, a complex flow occurs which leads to trapped strains and stresses. We expect coarsening to relax at least partially such macroscopic stresses, [21] in agreement with numerical simulations by Kermode reported in Ref. [2], as well as in recent experiment [22]. In addition to relaxing slowly macroscopic stresses, coarsening also creates stresses on the bubble scale which are intermittently released upon bubble rearrangements. Such stresses can be relaxed by controlled preshearing of the

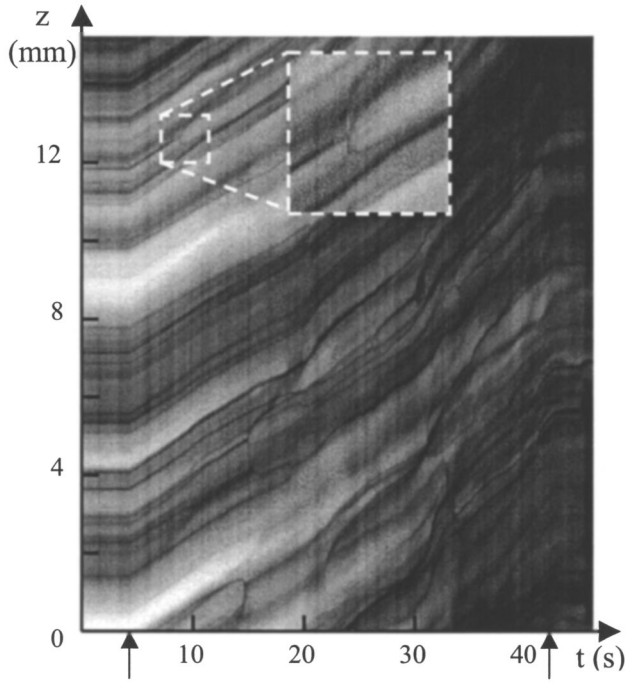

FIG. 3. Spatiotemporal plot generated for a pixel line located at $x=3.3$ mm. The gap width is $d=11.5$ mm and the shear rate is equal to 0.043 s^{-1}. The vertical and horizontal axes correspond, respectively, to the position in the shear direction z and to time t. The two arrows on the horizontal axis indicate the beginning and the end of shear. The inset shows a zoom on a kink due to a rearrangement.

sample [17,23] as will be discussed in the following.

The sliding plate cell (plane Couette geometry) consists of two vertical parallel glass plates (100×80 mm^2). To prevent wall slip, we use plates that are rough on the scale of about 1 mm and rendered hydrophobic using a chemical treatment. One plate is fixed, while the other can be moved in the z direction at a constant velocity V (cf. Fig. 1). This velocity can be chosen in the range from 0.02 to 3 mm/s. The gap between the plates, d, can be set to either 11.5 or 16.0 mm. The shear rate is defined as $\dot{\gamma}=V/d$. During a strain growth experiment, successive images of the deformed structure are recorded as the strain grows from 0 up to a maximum value 1.7. The image grabbing rate can be adjusted between 5 and 25 images per second. Such movies enable us to detect the onset of yielding in the sample, as well as to measure the velocity profile in the gap.

To measure the velocity in the z direction inside the foam, as a function of the distance x from the fixed plate, we generate spatiotemporal plots; pixel lines corresponding to a given value of x are extracted from successive images, and then juxtaposed to form the new plot (cf. Fig. 3). For immobile foam, one expects horizontal lines of constant brightness. If the evolution of the foam structure under steadily increasing shear were affine, one would expect space-time plots containing tilted straight lines of constant brightness with a slope equal to the local and instantaneous velocity $v_z(x,z,t)$. Nonaffine deformation of the foam structure leads to deviations from such a pattern. In particular, strain induced bubble rearrangements give rise to marked irregularities in the space-time plots that occur over a brief time interval (cf. Fig. 3).

To quantify the bubble flow induced by shearing, we determine a mean velocity in the z direction, $\overline{v}(x)$, averaged over a pixel line for a given value of x and over a time interval. Let us denote $I(x,z,t)$ the intensity of a pixel at a position (x, z) and at a time t in a spatiotemporal plot. We quantify the extent to which the evolution of a pixel line for a given value of x, during a time interval Δt, can be described as a translation Δz of the pixels in the z direction by calculating the correlation function $\langle I(x,z,t)I(x,z+\Delta z,t+\Delta t)\rangle_z$. The distance Δz corresponding to the strongest correlation is called $\Delta z_m(x,t)$. For each experiment, Δt has to be sufficiently short to resolve rapid structural changes such as rearrangements and long enough to obtain good precision in the measurement of Δz_m. As a compromise between these criteria, we choose $\Delta t=R/(2V)$. We thus obtain an estimate $\Delta z_m(x,t)/\Delta t$ of the instantaneous mean velocity. The time evolution of this quantity is studied by calculating its temporal average, denoted $\overline{v}(x)$, and the corresponding standard deviation. Using this procedure, we are able to establish the average foam velocity profile $\overline{v}(x)$, throughout the gap using a set of spatiotemporal plots for values of x ranging from 0 to d.

Moreover, in the aim to study the effect of strain history on the onset of yielding, we perform strain cycling experiments; upon each cycle, the sample is subjected to a strain that rises at a fixed rate $\dot{\gamma}$ up to a maximum value, denoted $\gamma_{\max}$, then stays constant for 1 s and finally comes back to zero strain. Up to three such cycles of equal maximum strain were applied successively to the sample, with strain rates ranging from 0.04 to 0.18 s^{-1}. We choose a fixed time interval of 1 min between the instants where the maximum strain is reached in successive cycles, whatever the maximum strain and the strain rate. This choice ensures that the total duration and, thus, the influence of coarsening is the same for all of the experiments. Before and after each cycle, images of the initial and final foam structures are recorded. They do not differ significantly in average and variance of intensity. Therefore, we quantify the extent of the irreversible structural changes induced by shearing using a correlation factor defined as follows:

$$C=\frac{\langle (A_i(x,z)-\langle A_i\rangle)(A_f(x,z)-\langle A_f\rangle)\rangle}{\langle (A_i(x,z)-\langle A_i\rangle)^2\rangle}. \qquad (1)$$

$A_i(x,z)$ and $A_f(x,z)$ are the intensities of pixels at the position (x, z) and the indices i and f distinguish between initial and final images. The angular brackets represent averages over the pixels. The correlation factor is 1 for identical initial and final images and it decreases as irreversible structural changes occur during the cycle.

III. RESULTS AND DISCUSSION

Figure 3 is a typical spatiotemporal plot obtained for a strain growth experiment. Up to the beginning of the shear deformation, the lines of constant brightness are horizontal

and continuous, indicating a static structure. Following the start of the strain growth, we observe a first regime where the lines are all tilted, continuous and parallel. Thus, the strain in the foam sample is to a good approximation homogeneous and there are not any topological changes of the bubble packing. Note that the nonaffine deformation that is known to exist at the scale of the individual films [7] is beyond the resolution of our experimental technique. Beyond a characteristic strain denoted γ_c, a second regime can be identified where kinks appear on the lines, indicating that the Plateau border displacement is no longer a smooth function of time; the kinks correspond to sudden topological transformations of the Plateau border network, as illustrated in Fig. 2(b). In principle, kinks in the spatiotemporal plots could also arise due to motions of bubbles in the x or y directions that are not directly related to topological rearrangements. We have verified experimentally that such effects are rare by comparing unprocessed images and spatiotemporal plots. Beyond a characteristic strain denoted by γ^* which is significantly larger than γ_c, a third regime progressively appears where the lines are neither continuous nor parallel, and their slopes differ from the one observed in the previous regimes, indicating nonaffine bubble motion that strongly fluctuates in space and time. γ^* presents extremely large fluctuations: In 30% of the experiments, it exceeded 1.7, the maximum strain applied to the samples. We choose not to extend the range of applied strains further, since due to the free lateral boundary conditions of the sample, a sliding plate configuration is intrinsically inadequate for applying very large fully homogeneous strains.

Figure 4 shows typical velocity profiles $\overline{v}(x)$ obtained for shear strain values in the three regimes. In all cases, the velocities of the bubbles in contact with the glass plates at $x=0$ and $x=d$ correspond to those of the respective plates, allowing to exclude artifacts related to wall slip. In the range of investigated shear rates, $\overline{v}(x)$ remains globally linear up to the strain value γ^*. This observation implies that for $\gamma_c < \gamma < \gamma^*$, the rearrangements are localized and randomly distributed in the sample. A direct study of the spatiotemporal plots such as Fig. 3 confirms this finding. Indeed, the signature of avalanchelike, large scale collective rearrangements would be kinks that simultaneously appear for a wide range of z. Visual inspection of the foam images shows that the extent in the x direction of bubble clusters undergoing rearrangements is comparable to that in the z direction. For strains beyond γ^*, the strain rate is no longer homogeneous throughout the foam. In this regime, we observe temporal fluctuations of the velocity $\overline{v}(x)$ that are much larger than for $\gamma < \gamma^*$. The profile and its fluctuation do not present any systematic variations with strain rate and gap size, within the investigated range of parameters.

To detect quantitatively the onset of yielding of the foam, corresponding to the passage from the first to the second regime defined above, we analyze spatiotemporal plots for a closely spaced set of x values ranging from 0 to d. To define γ_c precisely, we identify it with the strain at which the first rearrangement appears in these plots for a given experiment. Let us relate this parameter to the number of strain induced rearrangements per total sample volume, denoted ρ, which is

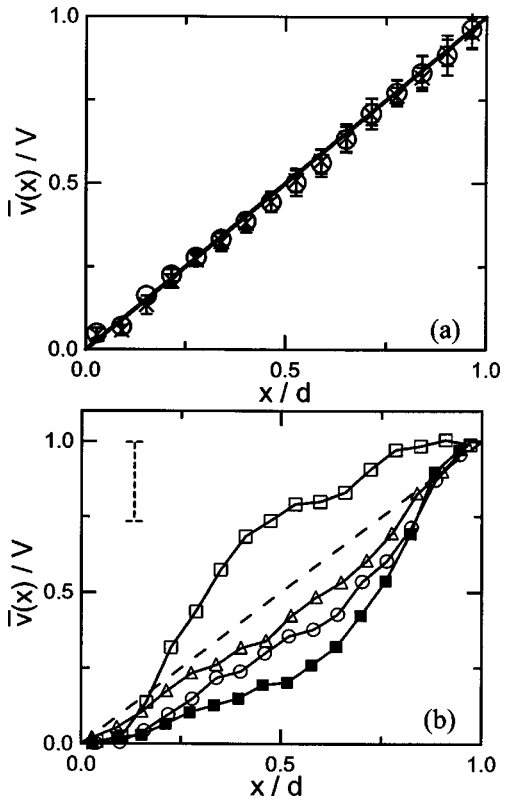

FIG. 4. Normalized velocity profiles $\overline{v}(x)/V$ for different shear strains and strain rates. (a) The symbols indicate the strain interval over which the data have been averaged; (○) $0<\gamma<\gamma_c$, (×) $\gamma_c<\gamma<\gamma^*$. The standard deviation of the strain dependent fluctuations of $\overline{v}(x)/V$ is indicated by the error bars. It is of the order of the experimental resolution. The straight line corresponds to the curve expected for uniform strain. The strain rate is 0.04 s^{-1}. Comparable results are obtained in the entire range of strain rates. (b) Velocity profiles averaged over the strain interval $\gamma^*<\gamma<1.7$. The symbols correspond to experiments with the following parameters: (○) $\dot{\gamma}=0.22\ s^{-1}$ and $\gamma^*=0.85$, (△) $\dot{\gamma}=0.14\ s^{-1}$ and $\gamma^*=0.76$, (□) $\dot{\gamma}=0.04\ s^{-1}$ and $\gamma^*=1$, (■) $\dot{\gamma}=0.03\ s^{-1}$ and $\gamma^*=0.60$. The gap width d is equal to 11.5 mm in all experiments except the one for $\dot{\gamma}=0.03\ s^{-1}$, where $d=16$ mm. The dashed straight line corresponds to uniform strain. Typical strain dependent fluctuation of $\overline{v}(x)/V$ is illustrated by an error bar drawn in the top left corner.

an increasing function of the applied strain and which we expect to be a bulk property of the foam for $\gamma<\gamma^*$. A simple statistical argument given in the Appendix allows to relate ρ to the probability p that no rearrangement occurs in the observed volume $V_{\rm obs}$ for strains up to γ: $\rho=-\ln[p]/V_{\rm obs}$. We estimate the strain γ for which $p=0.5$ as the average of γ_c, obtained in a set of experiments for a given strain rate $\dot{\gamma}$. In our experiments, we thus obtain a bulk density of rearrangements ρ equal to 1.7 cm^{-3}. To summarize this analysis, we note that the average value of γ_c corresponds to the average amount of strain that induces the onset of rearrangements, detected with a level of sensitivity of 1.7 rearrangements per cm^3.

In the previous discussion, we assumed that the first rearrangement observed during a shear start-up experiment is induced by the applied strain. However, this hypothesis is

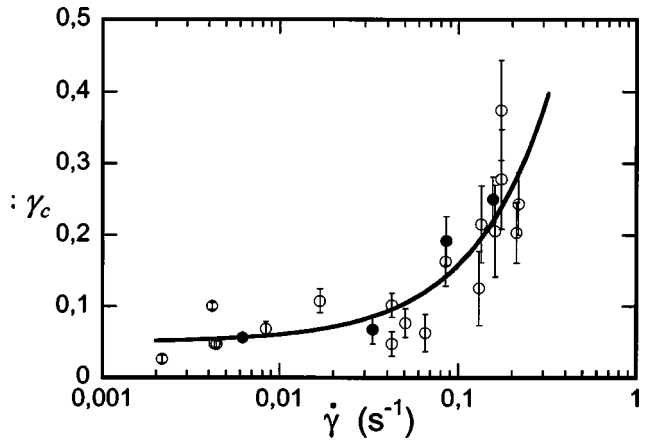

FIG. 5. Onset of yielding γ_c as a function of strain rate $\dot{\gamma}$. Open circles and disks correspond to experiments with a gap width equal to 11.5 mm and 16.0 mm, respectively. The continuous line corresponds to the fit explained in the text. Error bars indicate the measurement errors due to the finite image grabbing rate.

valid only if rearrangements due to the coarsening process are sufficiently rare; the number of such rearrangements detected in the observed volume per unit time, multiplied by $\gamma_c/\dot{\gamma}$ must be much smaller than one. This argument, based on the assumption that coarsening and strain induced rearrangements are independent phenomena, implies that we must restrict our study to strain rates much larger than 10^{-3} s^{-1}. To rule out artifacts related to the finite size of the sample, the measurements have been performed for two different gap widths; results are indeed independent of this parameter for a fixed amount of observed volume.

The data shown in Fig. 5 indicate that γ_c is nearly constant for low strain rates ranging from 0.002 to 0.07 s^{-1}. At higher strain rates, the onset of yielding occurs at strains γ_c that strongly increase with $\dot{\gamma}$. This evolution of the yield stress with strain rate can be understood qualitatively by noting that in the quasistatic limit, the stress is dominated by surface tension forces whereas at high strain rates, viscous stresses play an important role. We expect on dimensional grounds that the limit of the quasistatic regime should be governed by a characteristic capillary number $\mathrm{Ca}=\mu R\dot{\gamma}/\sigma$. This criterion should allow to compare yielding in foams of different liquid viscosity, surface tension, and bubble radius for a gas volume fraction comparable to that of our samples. Our experiments cover the range $7\times10^{-8}<\mathrm{Ca}<7\times10^{-6}$ with a crossover at a capillary number of the order of 2×10^{-6}. Previous rheological determinations of yield stresses and strains at well defined strain rates have generally been carried out at much lower capillary numbers, corresponding to the quasistatic regime [12]. This is consistent with the fact that yield strains and stresses have been reported to be independent of strain rate.

More insight is provided by the theoretical analyses by Khan and Armstrong [8] and Kraynik and Hansen [9] who used a model of film-level viscous flow to study simple shearing flow of perfectly ordered two-dimensional foams. They showed that the effect of viscous forces under steady shear is governed by a modified capillary number $\mathrm{Ca}'=\alpha\mu a(1-\phi)\dot{\gamma}/\sigma$, where a is the initial length of a cell side, ϕ the gas volume fraction, and α a geometrical prefactor of the order of 1. They further predicted that the most significant effect of the viscous forces consists in slowing down any length changes of the films separating bubbles. Thus, for high shear rates, bubbles will rearrange only after having reached very strong deformations. The yield strain γ_c is predicted to be independent of Ca' up to a characteristic value above which a rapid increase of γ_c with Ca' is expected. Furthermore, the cited theoretical studies present numerical values of $\gamma_c(\mathrm{Ca}')$ that may be described by a relation of the form $\gamma_c=\gamma_{c,o}+A\mathrm{Ca}'$, where $\gamma_{c,o}$ is the quasistatic limit of γ_c and $A\approx20$ is a dimensionless parameter. This expression is equivalent to $\gamma_c=\gamma_{c,o}+T\dot{\gamma}$, where T is a characteristic time. The fit in Fig. 5 shows that our data is in agreement with the expected functional relation with $\gamma_{c,o}=0.05\pm0.02$ and $T=1.08\pm0.14$ s. However, the prefactor A deduced from our experimental data exceeds the theoretical value by at least five orders of magnitude. This may partly be due to the fact that the theoretical model describes ordered 2D foam. In this context, new theoretical work taking into account mechanisms related to fluid flow in the vicinity of the Plateau borders [10], viscous flow along the Plateau borders which is specific to 3D foams as well as interfacial viscoelastic effects [24] would be of great interest. A better understanding of the maximum strain rate where yielding behavior is quasistatic is crucial for the comparison of experimental data with simulations obtained using the surface evolver software. Indeed, the results of this much used tool for theoretical investigations are only valid in the quasistatic regime [2,7]. Moreover, in applications of flowing foam such as mineral flotation [25], bubbles are of the order of a millimeter, and thus flow behavior at capillary numbers beyond the quasistatic regime is of great practical interest.

The quantitative comparison of our results concerning γ_c with rheological yield strain data is not straightforward, since there is at present no proven theory relating quantitatively the onset of structural changes to macroscopic rheological behavior. Yield strains for dry foams reported in the literature [8,14] strongly vary according to the experimental technique and yield criterion used, the values are in the range from 0.18 to 0.5. Surface evolver simulations of the yielding of dry 3D foams also give values in this range [26], even though systematic statistical studies to our knowledge have not yet been published in the literature. A fundamental problem for experimental as well as for numerical studies of yielding is the great variety of microstructures possible for a random foam. Surface evolver simulations of sheared 3D dry foams have recently shown that an ''annealed'' structure of decreased energy can be obtained by strain cycling of an amplitude large enough to provoke many rearrangements but small enough to prevent the buildup of residual stress [27]. We expect that prolonged coarsening can be considered as another way to obtain a statistically well defined distribution of internal strains that naturally appears in any sufficiently stable foam. The onset of yielding should be observed at much higher strains if annealed rather than coarsened foams are studied. To verify this prediction, we have carried out successive strain cycle experiments as described in Sec. II.

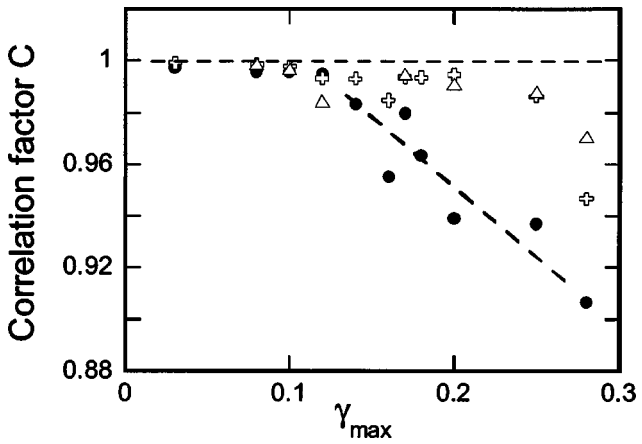

FIG. 6. The image correlation factor C [cf. Eq. (1)] is represented as a function of the maximum strain γ_{max} applied in a strain cycling experiment. C is measured for the first (disks), the second (crosses), and the third (triangles) of three successive cycles. The gap width is 11.5 mm, the strain rate is 0.18 s^{-1}.

Figure 6 shows image correlation factors that allow to compare the onset of irreversible changes induced by a first, a second, and a third shear cycle. The first cycle leads to irreversible rearrangements starting at deformation amplitudes in the range 0.1–0.15. Remarkably, the second as well as the third cycles do not induce a significant amount of further rearrangements below strain amplitudes of the order of 0.25. At larger strain amplitudes, all three cycles induce rearrangements. These findings concerning the interplay of strain history and yielding will help to guide the future development of mesoscopic foam rheology models.

IV. SUMMARY AND CONCLUSION

Using video observation of dry aqueous foams combined with spatiotemporal image analysis, we have studied the onset of yielding at the start up of a steady shear flow as a function of strain rate $\dot{\gamma}$. We have shown by direct observation in the bulk that the strain induced rearrangements that occur at small strains are distinct, localized events. In a range of strains extending well beyond the onset of yielding, we have explicitly verified that the bubble velocity profile in the gap is linear. For very large strains, fluctuating nonlinear profiles are found. Furthermore, we have observed a transition from a quasistatic regime at low $\dot{\gamma}$ to a regime where the onset of yielding occurs at strains that rapidly increase with $\dot{\gamma}$. These findings are in qualitative agreement with previous theoretical studies of viscous effects in 2D dry foams even though the underlying physical mechanism may not yet be well understood. Moreover, we have performed strain cycling experiments showing that the onset of rearrangements in a shear start-up flow strongly depends on strain history. Experimentally, reproducible histories may be obtained either by prolonged coarsening or by shear cycling, leading to onsets of yielding at widely differing strains.

ACKNOWLEDGMENTS

We thank A. Kraynik for fruitful discussions, S. Vincent-Bonnieu who carried out the strain cycling experiments in the framework of his DEA training, and D. Hautemayou for his technical help. This work was supported by the MENRT through the EA 2179 and by the CNES.

APPENDIX

Let us call $\delta\mathcal{V}$ a small element of the foam sample volume corresponding to the typical extent of structural changes observed upon a shear induced rearrangement and ρ the number of such rearrangements per volume. Since here, we are interested only in the onset of yielding, we restrict our discussion to the case $\rho\ \delta\mathcal{V} \ll 1$. Our observations show that ρ is independent of the position in the sample and we therefore describe shear induced rearrangements using a Poisson process in space. As a consequence, the probability x of not finding a rearrangement in the observed part of the sample volume V_{obs} is: $x=(1-\rho\ \delta\mathcal{V})^{\mathcal{V}_{obs}/\delta\mathcal{V}}$. Since $V_{obs} \gg \delta\mathcal{V}$, we obtain to a good approximation; $x=e^{-\rho\mathcal{V}_{obs}}$.

[1] R. G. Larson, *The Structure and Rheology of Complex Fluids* (Oxford University Press, Oxford, 1999), Chaps. 1 and 9.
[2] D. Weaire and S. Hutzler, *The Physics of Foams* (Clarendon Press, Oxford, 1999), Chaps. 1 and 8.
[3] H. M. Princen, J. Colloid Interface Sci. **91**, 160 (1983).
[4] P. Sollich, F. Lequeux, P. Hébraud, and M. E. Cates, Phys. Rev. Lett. **78**, 2020 (1997); P. Hébraud and F. Lequeux, *ibid.* **81**, 2934 (1998).
[5] T. Okuzono and K. Kawasaki, Phys. Rev. E **51**, 1246 (1995).
[6] D. J. Durian, Phys. Rev. E **55**, 1739 (1997); S. Tewari *et al.*, *ibid.* **60**, 4385 (1999).
[7] D. A. Reinelt and A. M. Kraynik, J. Fluid Mech. **311**, 327 (1996); J. Rheol. **44**, 453 (2000).
[8] S. A. Khan and R. C. Armstrong, J. Non-Newtonian Fluid Mech. **22**, 1 (1986); **25**, 61 (1987).
[9] A. M. Kraynik and M. G. Hansen, J. Rheol. **31**, 175 (1987).
[10] L. W. Schwartz and H. M. Princen, J. Colloid Interface Sci. **118**, 201 (1987).
[11] T. Okuzono, K. Kawasaki, and T. Nagai, J. Rheol. **37**, 571 (1993).
[12] S. A. Kahn, C. A. Schnepper, and R. C. Armstrong, J. Rheol. **32**, 69 (1988).
[13] B. S. Gardiner, B. Z. Dlugogorski, and G. J. Jameson, J. Rheol. **42**, 1437 (1998).
[14] A. Saint-Jalmes and D. J. Durian, J. Rheol. **43**, 1411 (1999).
[15] R. Höhler, S. Cohen-Addad, and A. Asnacios, Europhys. Lett. **48**, 93 (1999).
[16] A. D. Gopal and D. J. Durian, J. Colloid Interface Sci. **213**, 169 (1999).
[17] S. Cohen-Addad and R. Höhler, Phys. Rev. Lett. **86**, 4700 (2001).

[18] I. K. Ono, C. S. O'Hern, D. J. Durian, S. A. Langer, A. J. Liu, and S. R. Nagel, Phys. Rev. Lett. **89**, 095703 (2002).
[19] L. Cipelletti and L. Ramos, Curr. Opin. Colloid Interface Sci. **7**, 228 (2002).
[20] F. da Cruz, F. Chevoir, D. Bonn, and P. Coussot, Phys. Rev. E **66**, 051305 (2002).
[21] A. D. Gopal and D. J. Durian, e-print cond-mat/0208181.
[22] Y. Khidas, S. Cohen-Addad, and R. Höhler (unpublished).
[23] A. D. Gopal and D. J. Durian, Phys. Rev. Lett. **75**, 2610 (1995).
[24] D. M. A. Buzza, C.-Y. D. Lu, and M. E. Cates, J. Phys. II **5**, 37 (1995).
[25] See for instance, www.mimpt.com.au/jamesoncell-advantages.html
[26] A. M. Kraynik, D. A. Reinelt, and F. van Swol, in *Proceedings of the 3rd EuroConference on Foams, Emulsions and Applications*, edited by L. J. Z. Pacelli, J. Banhart, and G. L. M. M. Verbist (Verlag MIT, Bremen, 2000), p. 191.
[27] A. M. Kraynik, D. A. Reinelt, and F. van Swol (unpublished).